Extremely asymmetric electron localization in H_2^+ controlled with a THz field

Zhengmao Jia,[1] Zhinan Zeng,[1,*] Ruxin Li,[1,†] Zhizhan Xu,[1,‡] and Yunpei Deng[2]

[1]*State Key Laboratory of High Field Laser Physics, Shanghai Institute of Optics and Fine Mechanics, Chinese Academy of Sciences, Shanghai 201800, China*

[2]*Fritz-Haber-Institut der Max-Planck-Gesellschaft, Faradayweg 4-6, 14195 Berlin, Germany*

(Received 8 August 2013; published 18 February 2014)

We propose a scheme to achieve extremely asymmetric electron localization during molecular dissociations. Hydrogen molecular ion (H_2^+) dissociation is investigated theoretically. A THz pulse is used to steer the electron motion after the molecular ion is excited by an ultrashort ultraviolet laser pulse. A high probability, as high as 99.3%, to localize electrons on one of the two nuclei is demonstrated, with a dissociation probability of 6.14% and almost no ionization, by optimizing the peak intensities and time delay of the two pulses. Even when the total dissociation probability is increased to 25.6%, more than 96.3% electrons can be localized in all dissociation events. These results represent a significant advancement in the electronic dynamics control in molecules.

DOI: 10.1103/PhysRevA.89.023419 PACS number(s): 32.80.Rm, 33.80.Rv, 42.50.Hz, 42.65.Ky

I. INTRODUCTION

Coherent control of electrons and fragments in chemical reactions and photoelectron processes has attracted a great deal of interest [1–3]. One of the main goals has been to find a way to selectively break and form molecular bonds in photochemical reactions [4]. With the advent of new laser technologies, in particular the carrier envelope phase (CEP) stabilized few-cycle pulses and isolated subfemtosecond pulses, several control strategies have been proposed [5–14].

Being the simplest molecule, H_2^+ and its isotopes play an important role in the theoretical and experimental studies of electron localization in the dissociation of molecules. Coherent control with a two-color laser field over the asymmetry dissociation of HD^+ and H_2^+ was reported [15,16]. A shaped laser pulse was proposed to control the dissociation pathway of H_2^+ [17]. Compared with a single pulse, two sequential pulses were proven to locate more electrons on the selected pathway [18–21]. The combination of an ultraviolet (UV) pulse and a time-delayed near-infrared pulse was used to realize an electron localization probability on one of the two nuclei as high as 85% [18]. More recently, a similar electron localization probability was obtained by using two-color midinfrared and near-infrared laser pulses [21].

In this paper we propose a two-pulse scheme to significantly enhance the electron localization during molecular dissociations. We utilize a terahertz (THz) pulse [22–27] to steer the electron motion between the two protons after an ultrashort UV laser pulse is used to excite the electron wave packet onto the dissociative $2p\sigma_u$ state. Both the THz and UV pulses are linearly polarized. By adjusting the time delay and peak intensities of the two pulses, a probability as high as 99.3% to localize electrons on one of the two nuclei can be obtained, with a dissociation probability of 6.14% and almost no ionization. The electron localization probability can still be 96.3% even when the total dissociation probability reaches 25.6%.

*zhinan_zeng@mail.siom.ac.cn
†ruxinli@mail.shcnc.ac.cn
‡zzxu@mail.shcnc.ac.cn

II. SIMULATION MODEL AND THE PARAMETERS OF THE ELECTRIC FIELDS

We use a reduced-dimensional model for the H_2^+ molecular ion in the calculation. The molecular axis is assumed to be parallel to the polarization direction of the two laser fields. Then we can use the one-dimensional non-Born-Oppenheimer time-dependent Schrödinger equation (TDSE) to do the simulation [28,29]. The corresponding TDSE can be written as [$e = \hbar = m_e = 1$ in atomic units (a.u.), which are used throughout the paper unless otherwise stated] [29]

$$i\frac{\partial}{\partial t}\varphi(z,R;t) = H(z,R;t)\varphi(z,R;t), \tag{1}$$

where

$$H(z,R;t) = -\frac{1}{m}\frac{\partial^2}{\partial R^2} + \frac{1}{R} - \left(\frac{2m_p + m_e}{4m_p m_e}\right)\frac{\partial^2}{\partial z^2} + \left(1 + \frac{m_e}{2m_p + m_e}\right)z[E_1(t) + E_2(t - \Delta t)] - [1 + (z - R/2)^2]^{-1/2} - [1 + (z + R/2)^2]^{-1/2}, \tag{2}$$

where R is the relative internuclear distance, z is the electronic coordinate with respect to the center of mass of the two nuclei, and m_e and m_p are the electron and proton masses ($m_e = 1$ and $m_p = 1837$), respectively.

The UV pulse is defined as $E_2(t) = E_{20}\sin(\pi t/T_2)^2\sin(\omega_2 t)$, where T_2 is the total length of the pulse, i.e., 7.9 fs. The THz pulse is defined by the vector potential $A(t) = -E_{10}/\omega_1\sin(\pi t/T_1)^2\cos(\omega_1 t)$, where T_1 is the total length, one cycle of the THz pulse; then $E_1(t) = -\frac{\partial A(t)}{\partial t}$. The total simulation time is defined by t_{end}, which can be much longer than the THz pulse. For time beyond the total length of the THz pulse, the electric field is set to zero. Here Δt is the time delay between the two pulses, which is defined as the difference of the envelope peaks of the two electric fields.

The ground state of H_2^+ (the $1s\,\sigma_g$ state), obtained by the evolution of the field-free Schrödinger equation in imaginary time [30], is used as the initial wave function of the time-dependent evolution. Equation (1) is numerically solved on

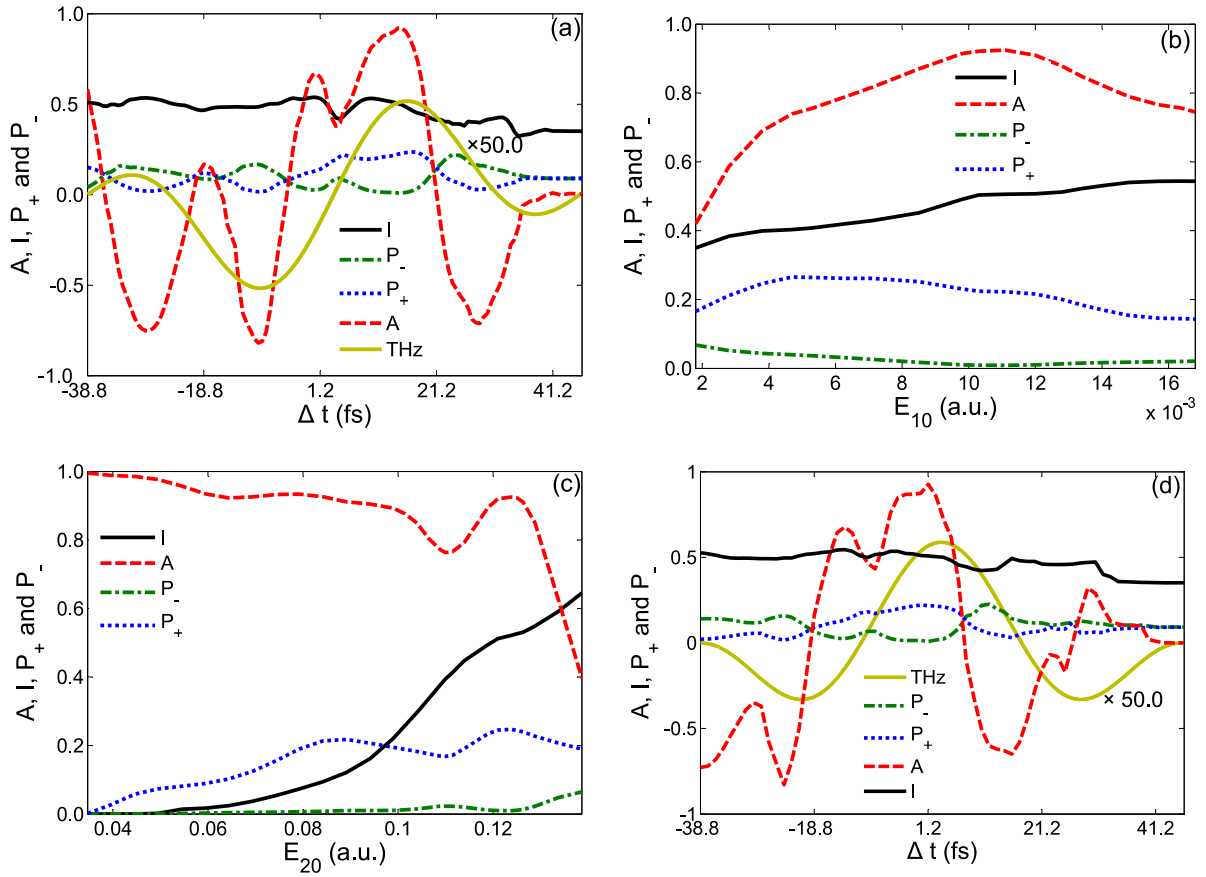

FIG. 1. (Color online) (a) Asymmetry parameter A, total ionization I, and $P_{\pm}$ as functions of time delay Δt. The intensities of the THz and UV pulses are 3.8×10^{12} and 5.0×10^{14} W/cm^2, respectively. The solid yellow curve is the electric field of the THz pulse. (b) Asymmetry parameter A, I, and $P_{\pm}$ as functions of the electric-field strength of the THz pulse E_{10}. The intensity of the UV pulse is 5.0×10^{14} W/cm^2 and $\Delta t =$ 14.6 fs. (c) Asymmetry parameter A, I, and $P_{\pm}$ as functions of the electric-field strength of the UV pulse E_{20}. The intensity of the THz pulse is 4.4×10^{12} W/cm^2 and time delay $\Delta t = 14.6$ fs. (d) Same as (a), but the CEP of the THz pulse is 0.5π.

a two-dimensional grid containing 8192 points on the z axis with a step of 0.3 a.u. and 1024 points on the R axis with a step of 0.1 a.u. The time step dt is set to 0.05 a.u. In order to avoid spurious reflections of the wave packets from the boundaries, a masking function $\cos^{1/8}$ is employed. We define the two channels of H_2^+ dissociation as [18,21,31]

$$P_{\pm} = \int_{10.0}^{R_{\max}} dR \int_{\pm R/2.0-5.0}^{\pm R/2.0+5.0} dz |\varphi(z, R; t_{\text{end}})|^2, \qquad (3)$$

where $R_{\max}$ corresponds to the boundary of the R axis and $\varphi(z, R; t_{\text{end}})$ is the final wave function of the system. In the simulation, $t_{\text{end}} = 106.8$ fs when $P_{\pm}$, the probabilities of the electron being localized on one of the protons (left – or right +), are stable.

In this simulation, the 228-nm UV pulse with an intensity of 5.0×10^{14} W/cm^2 and a pulse length T_2 of 7.9 fs is used to resonantly excite the electron wave packet onto the dissociative state $2p\sigma_u$. Then the 25.6-μm (11.7-THz frequency) THz pulse with an intensity of 3.8×10^{12} W/cm^2 and a pulse length T_1 of 85.3 fs (one-cycle) is used to steer the electron motion [32]. This THz pulse does not induce any further ionization. In the calculation, we set the dissociation asymmetry parameter as $A = (P_+ - P_-)/(P_- + P_+)$.

III. SIMULATION RESULTS AND DISCUSSION

Figure 1(a) shows A, the total ionization probability I, P_-, and P_+ as functions of Δt, the time delay between the UV and THz pulses. The intensities of the THz and UV pulses are $I_1 = 3.8 \times 10^{12}$ W/cm^2 and $I_2 = 5.0 \times 10^{14}$ W/cm^2, respectively. A large dissociation asymmetry parameter $A = 0.922$ can be obtained when $\Delta t = 14.6$ fs, which corresponds to an electron localization probability as high as 96.1% of all dissociation events. Because the UV pulse and the THz pulse overlap most of the time, the THz pulse will also work on the molecule and a transient heteronuclear molecule is thus formed when the UV pulse is used to excite the electron. That is why the ionization is asymmetric even during the UV pulse.

For curve A in Fig. 1(a), if we ignore the curve distortion around the delays of -18.8 and 3.2 fs, the whole curve is similar to the electric field of the THz pulse. The simulation shows that the damage of the electron localization around these two delays is due to the extraordinary electron excitations. Because of the dressing of the THz electric field, the electrons are not only excited onto the $2p\sigma_u$ state, but some are excited onto the higher state $3s\sigma$ around these delays by the UV pulse. Then the electron localization ratio is greatly decreased. Figure 1(d) is the same as Fig. 1(a) except that the CEP of the THz pulse is changed from 0.0 to 0.5π. Two points of damage

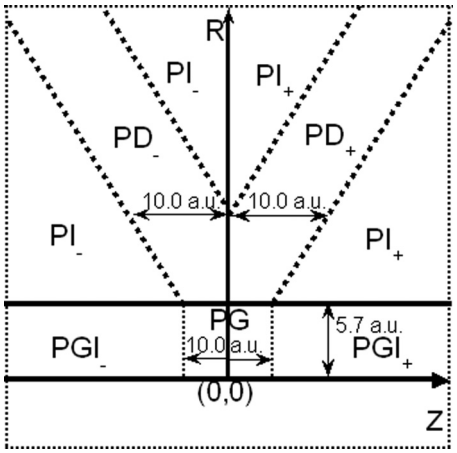

FIG. 2. Time-dependent electron probabilities of different parts.

can also be found on curve A, but they are around delays of -28.8 and -8.8 fs. It is also caused by the extraordinary electron excitations, as in Fig. 1(a). From Figs. 1(a) and 1(d) one can see that the waveform of the THz pulse greatly affects curve A. Thus the CEP of the THz pulse should be locked in the experiment.

Figure 1(b) shows A, I, and $P_{\pm}$ as functions of the strength of the THz field E_{10} at $\Delta t = 14.6$ fs and $I_2 = 5.0 \times 10^{14}$ W/cm^2. When the strength of the THz field is between 0.0071 a.u. (1.8×10^{12} W/cm^2) and 0.0134 a.u. (6.4×10^{12} W/cm^2), more than 90.0% of the electrons of the dissociative $2p\sigma_u$ state can be steered onto the right proton and the total dissociation probability is larger than 20.0%. When E_{10} is less than 0.0071 a.u., it is not high enough to ensure a good electron-direction selection. If E_{10} is higher than 0.0134 a.u., more electrons are excited onto the higher $3s\sigma$ state and the asymmetry parameter A decreases. Therefore, the THz pulse with peak intensity between 1.8×10^{12} and 6.4×10^{12} W/cm^2 can be used to control the electron localization.

Figure 1(c) depicts A, I, and $P_{\pm}$ as functions of the strength of the UV field E_{20} at $\Delta t = 14.6$ fs and $I_1 = 4.4 \times 10^{12}$ W/cm^2. When E_{20} is low, a large localization probability can be obtained with almost zero ionization and small dissociation probability. For example, when $E_{20} = 0.0446$ a.u., $A = 0.986$, the electron localization probability can be 99.3%, and the dissociation probability is 6.14%, with almost no ionization

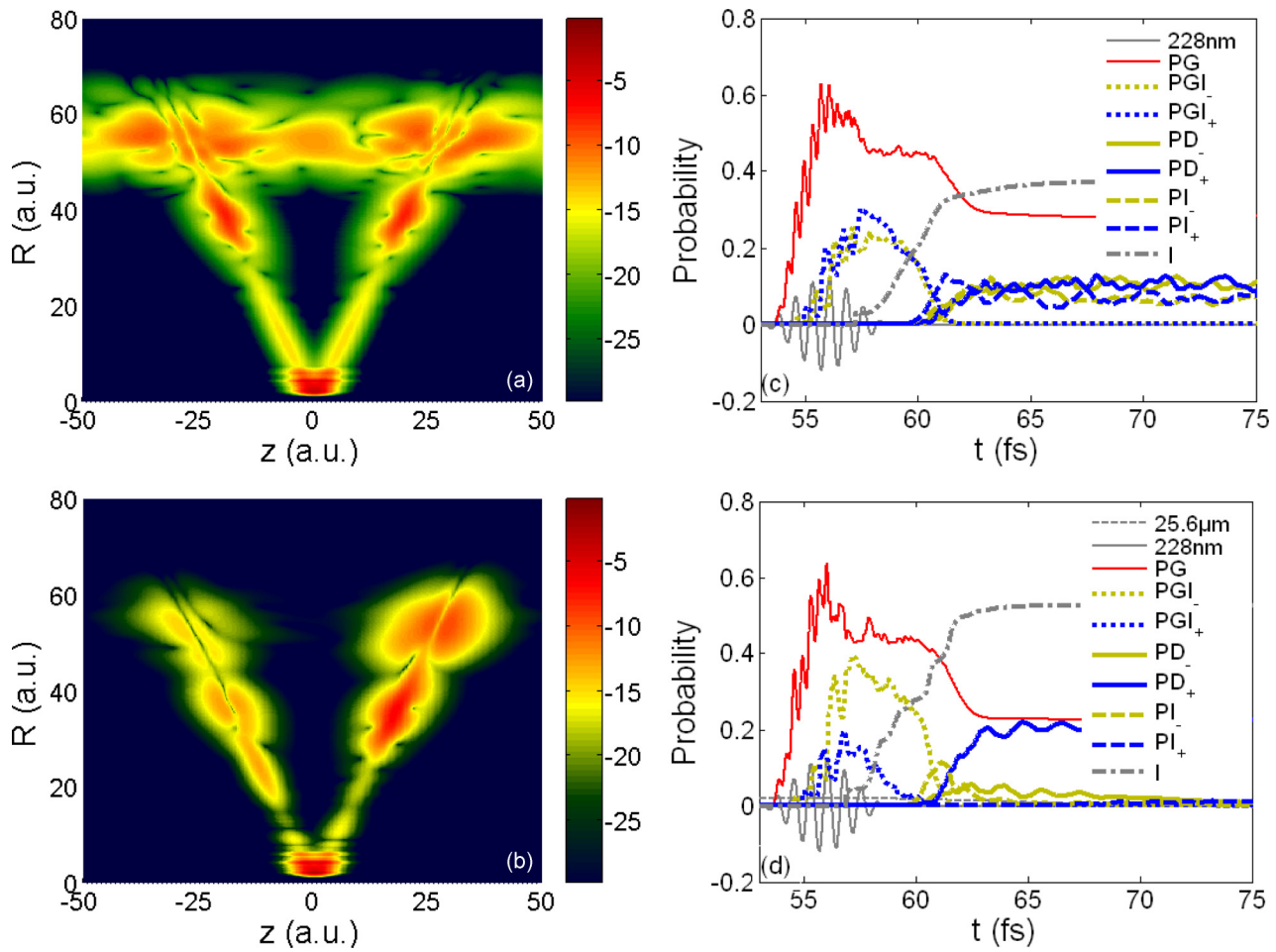

FIG. 3. (Color online) (a) and (b) Snapshots of the common logarithm of the electron-nuclear probability density distribution taken at $t = 106.8$ fs. (c) and (d) Time-dependent electron probabilities of $\mathrm{PD}_{\pm}(t)$, $\mathrm{PI}_{\pm}(t)$, $\mathrm{PG}(t)$, and $\mathrm{PGI}_{\pm}(t)$ and the total ionization probability I, respectively. (a) and (c) Only the UV laser pulse is applied. (b) and (d) Both the UV and THz pulses are applied with intensities of 3.8×10^{12} and 5.0×10^{14} W/cm^2, respectively, and time delay $\Delta t = 14.6$ fs.

(less than 0.0013%). With an increase of E_{20}, P_+ increases, but P_- and I increase too. For example, when $E_{20} = 0.124$ a.u., we find that $P_+ = 0.246$, $P_- = 0.096$, $A = 0.926$, and the total ionization probability $I = 0.521$. The total dissociation probability is increased to 25.6% and more than 96.3% of the electrons of the dissociative event can still be steered onto the right proton.

To reveal the details of the electron localization control, we define the time-dependent electron probabilities of different parts: $\mathrm{PD}_\pm$ for the electrons localized on the right (or left) proton, PG for the electrons of high vibrational bound states, and $\mathrm{PGI}_\pm$ and $\mathrm{PI}_\pm$ for the ionized electrons of the six sections, respectively, as depicted in Fig. 2. In this part, the intensities of the UV pulse and THz pulse are the same as those of Fig. 1(a): 5.0×10^{14} and 3.8×10^{12} W/cm^2, respectively.

Figures 3(a) and 3(b) show snapshots of the common logarithm of the electron-nuclear probability density distribution taken at the end of the simulation ($t_{\mathrm{end}} = 106.8$ fs) obtained without and with the THz pulse, respectively. One can find that the electron localization starts from about $R = 5.7$ a.u. Thus we use $R_0 = 5.7$ a.u. in the definition of $\mathrm{PD}_\pm$, which is a little different from the previous work and the $P_\pm$ above. From Fig. 3(a) one can see that if there is no THz pulse, a single UV pulse induces a symmetric electron distribution; however, when the THz pulse is employed, the symmetric distribution is seriously broken, as can be seen in Fig. 3(b). Further investigation shows that the CEP of the UV pulse will not generate a significant difference because it is a one-photon process. The stripe in Fig. 3(a) can be seen because the data are logarithmic, but the value is very small. Most of these electrons are in the high excited states; only the electrons between two nuclei (around $z = \pm 15$ a.u. and 45 a.u. $< R <$ 65 a.u.) can be thought of as ionized electrons. This is because the UV pulse is strong in the calculation. Although most of the electrons are excited onto the $2p\sigma_u$ state, some are still ionized or excited onto higher-energy states. For these states, the protons will have larger kinetic energy and appear at larger R positions.

The temporal evolution of the electron probabilities of different parts is presented in Figs. 3(c) (without a THz pulse) and 3(d) (with a THz pulse). Before the UV pulse is employed, all curves are almost zero, which means that the THz pulse itself cannot induce any ionization or dissociation. When the UV pulse is applied, the electron is first excited [the ground-state component PG(t) has been removed]. Then some electrons are ionized $\mathrm{PI}_\pm(t)$ (both curves are almost the same if there is no THz pulse [Fig. 3(c)], but different when a THz pulse is used [Fig. 3(d)]). If there is no THz pulse, the profiles of $\mathrm{PD}_\pm(t)$ are almost the same (about 0.1). When the THz pulse is employed, the maximum value of $\mathrm{PD}_-(t)$ [at about 63 fs in Fig. 3(d)] is decreased to be about 0.05, while $\mathrm{PD}_+(t)$ can be about 0.2. Compared to Fig. 3(c), some of the ionized electrons $\mathrm{PI}_-(t)$ can be pulled back to the proton by the THz pulse, which makes $\mathrm{PD}_+(t)$ larger in Fig. 3(d) than in Fig. 3(c). After that, the electrons on the left proton PD_- are further steered to the right proton PD_+ by the THz pulse until less than 1% of the electrons are left. When the probabilities of electrons localized on the protons (right or left) are stable, we can obtain $\mathrm{PD}_+ = 0.2244$ and $\mathrm{PD}_- = 0.0092$, respectively. Thus 96.07% of the electrons of the dissociation events are localized on the right proton. In these two cases, the total ionization ratios are about 35% (without a THz pulse) and 45% (with a THz pulse), respectively.

IV. SIMULATION WITH COUPLED EQUATIONS

The key role the THz pulse plays in the dissociation of H_2^+ ion can be explained as follows. In previous two-pulse schemes, the delayed pulse should induce single-photon coupling between the upper and lower states to achieve the electron localization. However, the photon energy of the THz pulse is too low to induce single-photon coupling between two states. So we further simulate with the coupled equations [33]

$$i\frac{\partial}{\partial t}\begin{pmatrix}\psi_g(R,t)\\ \psi_u(R,t)\end{pmatrix} = \begin{pmatrix}-\frac{1}{m_p}\frac{\partial^2}{\partial R^2} + V_g(R) & V_{gu}(R,t)\\ V_{gu}(R,t) & -\frac{1}{m_p}\frac{\partial^2}{\partial R^2} + V_u(R)\end{pmatrix} \times \begin{pmatrix}\psi_g(R,t)\\ \psi_u(R,t)\end{pmatrix}, \tag{4}$$

where $\psi_g(R,t)$, $\psi_u(R,t)$, $V_g(R)$, and $V_u(R)$ are nuclear wave packets of $1s\sigma_g$ and $2p\sigma_u$, the binding potential curve and the dissociative curve, respectively, and $V_{gu}(R,t)$ denotes the interaction of the external laser field. When the electron localization is considered, the nuclear wave packets on the right ψ_r and left ψ_l protons can be written as

$$\begin{aligned}\psi_r(R,t) &= \frac{1}{\sqrt{2}}[\psi_g(R,t) + \psi_u(R,t)],\\ \psi_l(R,t) &= \frac{1}{\sqrt{2}}[\psi_g(R,t) - \psi_u(R,t)].\end{aligned} \tag{5}$$

Then we can rewrite Eq. (4) with this representation as

$$\begin{aligned}i\frac{\partial}{\partial t}\psi_r &= \left[-\frac{1}{m_p}\frac{\partial^2}{\partial R^2} + \frac{V_g(R)+V_u(R)}{2} + V_{gu}(R,t)\right]\psi_r + \left[\frac{V_g(R)-V_u(R)}{2}\right]\psi_l,\\ i\frac{\partial}{\partial t}\psi_l &= \left[\frac{V_g(R)-V_u(R)}{2}\right]\psi_r + \left[-\frac{1}{m_p}\frac{\partial^2}{\partial R^2} + \frac{V_g(R)+V_u(R)}{2} - V_{gu}(R,t)\right]\psi_l.\end{aligned} \tag{6}$$

In Eq. (6) the electron jumping between two protons $\langle\psi_r|V_I^{rl}|\psi_l\rangle$ is decided by the interaction potential $V_I^{rl} = \frac{V_g(R)-V_u(R)}{2}$. However, V_I^{rl} is independent of the external laser field and decreases very fast (almost e^{-R} for large R) with an increase of the internuclear distance R. In this simulation, a Gaussian-type wave packet is pre-excited onto the dissociative state ψ_u with center position $R = 3.3$ a.u. (resonant with the 228-nm pulse). The waveform of the electric field used in the simulation is the same as that of the THz pulse mentioned above, but the wavelength and the intensity can be adjusted.

In Fig. 4(a) the time-dependent probabilities of different states are shown. The integrations for $\int|\psi_r|^2 dR$ and

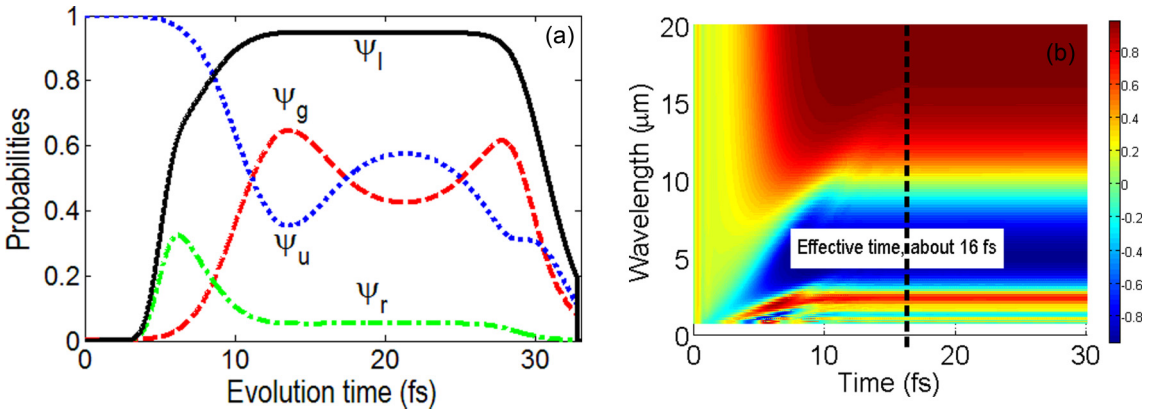

FIG. 4. (Color online) (a) Calculated results with coupled equations (4). The probability of electron localization is stable after about 12 fs, although the probabilities of ψ_g and ψ_u are still being exchanged. After about 28 fs, the nuclear wave packet reaches the boundary and is absorbed by the mask function. (b) Asymmetry parameter changing with different wavelengths. The electron is excited at $t = 0$. The pulse is a multicycle cosine function. From the figure we can see that, even though the pulse is very long, all the asymmetry parameters become stable at about 16 fs. The sine function pulse can obtain similar results.

$\int |\psi_l|^2 dR$ start from $R = 5.7$ a.u., so they are zero at first. The curves of $\int |\psi_r|^2 dR$ and $\int |\psi_l|^2 dR$ in Fig. 4(a) are almost the same as the curves $\mathrm{PD}_{\pm}(t)$ during the evolution time from about 60 to 75 fs in Fig. 3(d). After about 12 fs, the probabilities of $\int |\psi_r|^2 dR$ and $\int |\psi_l|^2 dR$ are stable, although the probabilities of the lower state ψ_g and the upper state ψ_u are still changing. That is because the phases of the states ψ_r and ψ_l are still changing (affected by the THz pulse). When the THz pulse ends, the oscillation of the states ψ_g and ψ_u will also stop.

Then why is the long-wavelength THz pulse used? The time-dependent asymmetry parameter A vs the wavelength of the steering pulse is shown in Fig. 4(b). In this simulation, a Gaussian-type wave packet is pre-excited onto the dissociative state ψ_u at $t = 0$ and then a multicycle pulse (the cosine function pulse is used here, while the sine function pulse leads to a similar result) is used to control the electron motion. As one can see, although the pulse is very long, all the asymmetry parameters A are stable after about 16 fs. That is to say, there is an effective time for the external field to control the electron localization within the H_2^+ dissociation. Further investigation shows that if the mass of the molecule is larger, the effective time is longer. When the period of the steering pulse is much shorter than the effective time, the oscillation of the asymmetric parameter can be seen. Although high electron localization can also be achieved at some special delay for the short-wavelength pulse, it is much easier for a long-wavelength one when the oscillation disappears. Moreover, with a longer-wavelength pulse, high electron localization can be achieved at a lower intensity, corresponding to a lower ionization ratio. However, a too-long wavelength means a waste of the pulse energy beyond the effective time. The half period of the steering pulse should match the effective time of the target molecule. Because the effective time is tens of femtoseconds for most of the molecules, using a THz pulse is therefore an applicable way to control their dissociation.

The work of the THz pulse, however, still needs further investigation. With Eq. (6), we know that the THz electric field affects the phase evolution of the states. In this representation, the electron jumping between two states ψ_r and ψ_l can be calculated with $\langle \psi_r | V_I^{rl} | \psi_l \rangle$. The THz electric field will affect the phase evolution of the states as $\pm \int V_{gu}(R,t)dt$. The phase difference between the two states decides the direction of the electron jumping, so it will be affected by the wavelength and intensity of the THz pulse.

This, however, does not mean that the THz pulse works as a static electric field. If the strength of a static electric field is strong enough, it can act partly as a THz pulse. The static electric field can increase the electron localization ratio greatly and the required strength should be higher than 10.0 MV/cm. Even so, the static electric field is still not as effective as the THz pulse. We have performed the simulation to compare the static electric field with the THz pulse and found that the THz pulse would do better. According to our simulation, $A = 1$ can be achieved very easily in the simulation with Eq. (4), but it is impossible in the simulation with a TDSE because of the multistate excitation and ionization. The time delay between the UV pulse and the THz pulse will help to optimize the electron localization. However, for static electric field, we can only change its strength: It is not good enough.

V. SUMMARY

In conclusion, we have shown that the extremely high degree of electron localization in the dissociation of the H_2^+ ion can be achieved by using the two laser pulses of UV and THz spectral regimes. A high localization probability of 99.3% has been demonstrated, while the dissociation probability is 6.14% and the ionization probability is almost zero (less than 0.0013%). A high localization probability of 96.3% can also be achieved with a higher dissociation probability of 25.6%, while the ionization probability is also very large. The simulation with coupled equations shows that there is an effective time for the controlling the electron localization, in favor of a long-wavelength laser pulse. For the H_2^+ ion, this effective time is about 16 fs (with the classical simulation, it needs

18.27 fs for the proton to reach $R = 10$ a.u.). If the laser wavelength is long enough, the requirement for the intensity of the controlling pulse can be very low, leading to very low ionization probability. Thus the proposed scheme enables the approach to efficiently control the electron localization during the molecular dissociation.

ACKNOWLEDGMENTS

This work was supported by NSF (Grants No. 11127901, No. 60921004, No. 11134010, No. 11222439, No. 11227902, and No. 61108012) and the 973 Project (No. 2011CB808103) of China.

[1] T. Brixner and G. Gerber, Chem. Phys. Chem. **4**, 418 (2003).
[2] P. Lan, P. Lu, W. Cao, Y. Li, and X. Wang, Phys. Rev. A **76**, 011402 (2007).
[3] A. González-Castrillo, A. Palacios, H. Bachau, and F. Martín, Phys. Rev. Lett. **108**, 063009 (2012).
[4] A. H. Zewail, J. Phys. Chem. A **104**, 5660 (2000).
[5] T. Babrec and F. Krausz, Rev. Mod. Phys. **72**, 545 (2000).
[6] F. Lindner, M. G. Schätzel, H. Walther, A. Baltuška, E. Goulielmakis, F. Krausz, D. B. Milošević, D. Bauer, W. Becker, and G. G. Paulus, Phys. Rev. Lett. **95**, 040401 (2005).
[7] V. Roudnev, B. D. Esry, and I. Ben-Itzhak, Phys. Rev. Lett. **93**, 163601 (2004).
[8] M. F. Kling, Ch. Siedschlag, A. J. Verhoef, J. I. Khan, M. Schultze, Th. Uphues, Y. Ni, M. Uiberacker, M. Drescher, F. Krausz, and M. J. J. Vrakking, Science **312**, 246 (2006).
[9] S. Chelkowski, G. L. Yudin, and A. D. Bandrauk, J. Phys. B **39**, S409 (2006).
[10] I. Znakovskaya, P. von den Hoff, G. Marcus, S. Zherebtsov, B. Bergues, X. Gu, Y. Deng, M. J. J. Vrakking, R. Kienberger, F. Krausz, R. de Vivie-Riedle, and M. F. Kling, Phys. Rev. Lett. **108**, 063002 (2012).
[11] D. Geppert, P. von den Hoff, and R. de Vivie-Riedle, J. Phys. B **41**, 074006 (2008).
[12] V. Roudnev and B. D. Esry, Phys. Rev. Lett. **99**, 220406 (2007).
[13] G. Sansone, F. Kelkensberg, J. F. Pérez-Torres, F. Morales, M. F. Kling, W. Siu, O. Ghafur, P. Johnsson, M. Swoboda, E. Benedetti, F. Ferrari, F. Lépine, J. L. Sanz-Vicario, S. Zherebtsov, I. Znakovskaya, A. L'Huillier, M. Yu. Ivanov, M. Nisoli, F. Martín, and M. J. J. Vrakking, Nature (London) **465**, 763 (2010).
[14] T. Rathje, A. M. Sayler, S. Zeng, P. Wustelt, H. Figger, B. D. Esry, and G. G. Paulus, Phys. Rev. Lett. **111**, 093002 (2013).
[15] B. Sheehy, B. Walker, and L. F. DiMauro, Phys. Rev. Lett. **74**, 4799 (1995).
[16] E. Charron, A. Giusti-Suzor, and F. H. Mies, Phys. Rev. Lett. **71**, 692 (1993).
[17] C. Lefebvre, T. T. Nguyen-Dang, and O. Atabek, Phys. Rev. A **75**, 023404 (2007).
[18] F. He, C. Ruiz, and A. Becker, Phys. Rev. Lett. **99**, 083002 (2007).
[19] F. He, A. Becker, and U. Thumm, Phys. Rev. Lett. **101**, 213002 (2008).
[20] F. He, Phys. Rev. A **86**, 063415 (2012).
[21] K. Liu, Q. Zhang, and P. Lu, Phys. Rev. A **86**, 033410 (2012).
[22] H. Hirori, A. Doi, F. Blanchard, and K. Tanaka, Appl. Phys. Lett. **98**, 091106 (2011).
[23] A. Sell, A. Leitenstorfer, and R. Huber, Opt. Lett. **33**, 2767 (2008).
[24] C. P. Hauri, C. Ruchert, C. Vicario, and F. Ardana, Appl. Phys. Lett. **99**, 161116 (2011).
[25] X. Xie, J. Dai, and X.-C. Zhang, Phys. Rev. Lett. **96**, 075005 (2006).
[26] Y. Bai, L. Song, R. Xu, C. Li, P. Liu, Z. Zeng, Z. Zhang, H. Lu, R. Li, and Z. Xu, Phys. Rev. Lett. **108**, 255004 (2012).
[27] J. Wu, Y. Tong, M. Li, H. Pan, and H. Zeng, Phys. Rev. A **82**, 053416 (2010).
[28] Y. Zheng, Z. Zeng, R. Li, and Z. Xu, Phys. Rev. A **85**, 023410 (2012).
[29] S. Chelkowski, A. D. Bandrauk, A. Staudte, and P. B. Corkum, Phys. Rev. A **76**, 013405 (2007).
[30] Z. Zeng, R. Li, W. Yu, and Z. Xu, Phys. Rev. A **67**, 013815 (2003).
[31] K. Liu, W. Hong, Q. Zhang, and P. Lu, Opt. Express **19**, 26359 (2011).
[32] S. Fleischer, Y. Zhou, R. W. Field, and K. A. Nelson, Phys. Rev. Lett. **107**, 163603 (2011).
[33] M. F. Kling, Ch. Siedschlag, I. Znakovskaya, A. J. Verhoef, S. Zherebtsov, F. Krausz, M. Lezius, and M. J. J. Vrakking, Mol. Phys. **106**, 455 (2008).